# Time-Reversal Imaging and Field-Separation-Method applied to the study of the Steelpan radiation

Eric Bavu, Clément Auzou, Mélodie Monteil, Manuel Melon, Christophe Langrenne, Alexandre Garcia

ACOUSTICS 2012

# Time-Reversal Imaging and Field-Separation-Method applied to the study of the Steelpan radiation

E. Bavu[a], C. Auzou[a], M. Monteil[b,c], M. Melon[a], C. Langrenne[a] and A. Garcia[a]

[a]Conservatoire National des Arts et Métiers, 292 rue Saint-Martin 75141 Paris Cedex 03
[b]IJLRDA-UPMC, 4 place jussieu, 75005 Paris, France
[c]UME (Unité de Mécanique), ENSTA - ParisTech, Chemin de la Hunière, 91761 Palaiseau, France
eric.bavu@cnam.fr

Time-reversal (TR) is a powerful method for the imaging and localization of sound sources. We propose the use of TR imaging in conjunction with a field separation method (FSM) in order to study the radiating sources of a steelpan. The TR-FSM method consists in measuring the acoustic pressure on a double-layer hemispherical time-reversal mirror (TRM). Outgoing waves are separated from ingoing waves by using spherical-harmonic expansions. The outgoing contribution is then time-reversed and numerically back-propagated, allowing to achieve accurate imaging of acoustically radiating sources. This FSM also allows to separate contributions from noise sources outside the region of interest (ROI), thus isolating the contributions from zones on the instrument. In this study, this imaging method is used for the imaging of radiating sources on a steelpan played by a performer. The results show that in some cases, the main contribution to the radiation comes from zones that were not mechanically excited by the panist.

# 1 Introduction

The Caribbean steelpan is one of the most recent hand-crafted idiophone, which was developed in the last century. The modern steelpan family covers a five-octave range, and is composed by several overlapping frequency range instruments: tenor, double-tenor, double-second, guitar, cello, quadrophonic, and bass [1]. In this paper, the study and measurements are achieved on the right drum of a double-second steelpan composed of 19 individual notes, whose pitch extends from $F3$ (174 Hz) to $F6$ (1397 Hz) (Fig. 1).

This instrument is a tuned idiophone whose sound is produced by the physical impact of playing sticks on the notes, whose vibrational behaviours can be modelized as thin metallic shells [2]. Tuners generally tune one mode an octave above the fundamental and a third mode a twelfth or two octaves above the fundamental [1]. Its mechanical and acoustical behaviour have been studied over the last decades by several authors [3, 4, 5, 6] and can be described as a system of mode-localized oscillators.

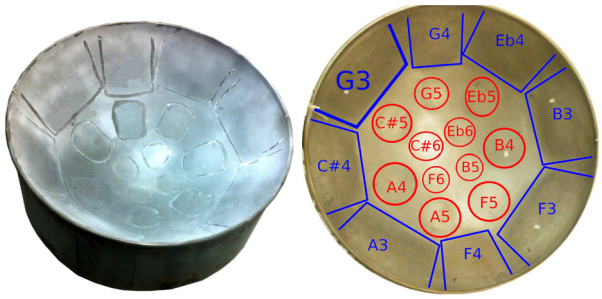


(a) (b)

Figure 1: (a) Studied double-second right drum - (b) Localization of notes. Red zones are the notes studied in this paper. Blue zones are the notes outside of the ROI

Besides radiating sound from the note struck with the stick, a steelpan radiates sympathetically from neighbouring notes and from the skirt [4]. Most of the studies on the steelpan radiation and vibration involve a sinusoidal excitation using a small magnet attached to the instrument near notes, driven by a harmonic magnetic field. Most of the authors measured the radiated field using holography [1], or nearfield acoustic holography (NAH) [7].

Although, the rich distinctive nature of the steelpan radiated sound is characterized by sympathetic vibrations and non-linear mode-localized oscillators [8] that interact via parametric internal resonances depending on the linear frequencies of the higher modes [2]. This results in amplitude and frequency modulations that are audible and constitutes a strong acoustic signature of the steelpan radiation. This behaviour is enhanced by the physical impact of the playing stick on the instrument.

Therefore, we propose an acoustic imaging method in order to visualize the zones of the instrument's bowl involved in the acoustic radiation when played by a performer with a stick. Recently, Woods *et al.* [9] proposed a conformal laser doppler vibrometry method in order to visualize the note areas that respond when adjacent or non-adjacent musically related notes are struck. Woods *et al.* [9] clearly illustrate the complex vibration of the steelpan and the *mechanical* coupling between notes but do not demonstrate the *acoustic radiation* induced by this complex vibration. The present paper aims at supplying some of this missing information on the acoustic radiation.

The present study focuses on the assessment of the bowl's acoustic radiation when the instrument is struck with a playing stick by a confirmed panist. In this paper, on contrary to several other published works, we do not intend to assess the whole instrument radiation, since the TR-FSM method allows to suppress the acoustic field contribution coming from the steelpan skirt. We only studied the 11 highest pitch notes, localized on the center of the bowl, represented by the red coloured zones on Fig. 1. We propose an acoustical imaging method based on time-reversal (TR) and a field separation method (FSM) using a double-layered hemispherical time-reversal mirror (Fig. 2) in order to assess the zones of the steelpan's bowl that predominantly contribute to the acoustic radiation of the instrument.

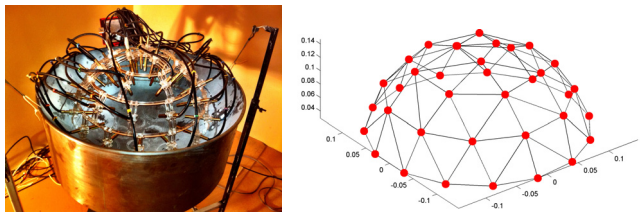

(a) (b)

Figure 2: (a) Double-layered hemispherical TRM placed on the steelpan in a reverberating room - (b) Geometry of the TRM: red dots represent the position of each pressure-pressure (p-p) probes on the antenna

Since the TR-FSM method allows to suppress the contributions coming from outside ROI located under the TRM and "dereverberates" the measured data [10], there is no need to achieve the acoustic pressure measurement in an anechoic room. Details on the sonic time-reversal imaging process, the field separation method, experimental methods, and the acoustic imaging results are given in the following sections.

# 2 Material and experimental methods

In all experiments presented in this paper, the steelpan is struck with a playing stick by a confirmed panist (M. Monteil) in a right-angled trapezium-shaped reverberating room (surface: 20,8 $m^2$, volume: 63 $m^3$, reverberation duration $T_R \geq 4.5$ s).

The pressure measurement array is a double-layered hemispherical time-reversal mirror (Fig. 2) made-up of 36 p-p probes (Fig. 3) manufactured by CTTM, thus giving access to 72 acoustic pressure measurements over time. The two hemispherical measurement layers formed by the p-p probes are spaced by 3 cm, the internal layer having a radius $a_1$ = 14.5 cm and the external layer having a radius $a_2$ = 17.5 cm. The antenna, formed by these 36 phase and amplitude-calibrated p-p probes (Fig. 3) is placed on the steelpan's bowl (Fig. 2(a)).

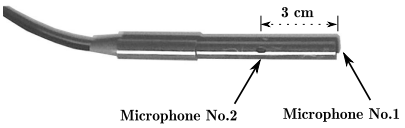


Figure 3: Pressure-pressure probe used in the TRM

Only the 11 highest pitch notes (ranging from A4: 440 Hz to F6: 1397 Hz) - represented in red coloured zones on Fig. 1- are under the TRM, noted as the region of interest (ROI). Each of these 11 notes is striked 5 times by the player in order to test the source localization reproducibility and the dependence of radiating sources on strike velocity level. Since the TRM is located on the top of the instrument, the player strikes each individual notes from the bottom of the bowl with the playing stick, without modifying the mechanical vibration and sound radiation of the instrument, though slightly altering the classical instrumental gesture.

The 72 synchronized time-pressure measurements are acquired and triggered through a National Instruments® 96 channel PXI acquisition system, sampled at 32768 Hz and driven using Labview® software. Calculation of TR imaging and acoustic field separation is achieved using Matlab® software.

# 3 Theoretical background

## 3.1 Sonic time-reversal imaging

Time-reversal (TR) is a powerful method for the imaging and localization of sound sources with high accuracy both in time and space domains [11, 12]. This imaging method is based on time-reversal invariance of the wave equation in weakly-dissipative media [11, 13]. This time-reversal invariance ensures that if an acoustic pressure field $p(\vec{r},t)$ is solution of the wave equation, the time-reversed acoustic field $p(\vec{r},-t)$ has a mathematical and physical existence. A time-reversed pressure field $p_{TR}(\vec{r},t)$ can be reconstructed at position $\vec{r} \in (V)$ using a time-reversed version of the time domain Helmholtz-Kirchhoff equation (1) and measurements of the acoustic pressure and its normal derivative on points $\vec{s}$ on a surface $(S)$ surrounding the volume $(V)$ where the calculation is done to retrieve the pressure field:

$$p_{TR}(\vec{r},t) = \iint_S \left( G(\vec{s},\vec{r};-t) * \frac{\partial p(\vec{s};-t)}{\partial n_s} - \frac{\partial G(\vec{r_s},\vec{r};-t)}{\partial n_s} * p(\vec{s};-t) \right) \cdot dS \tag{1}$$

The time-reversed field $p_{TR}(\vec{r},t)$ has the property to back-propagate to the acoustic sources and to reconstruct the time evolution of the radiated field at focal point, thus allowing to solve the inverse problem of acoustic field reconstruction and to locate and image acoustic radiating sources. Assuming that the measurement is achieved in free-field conditions, the free-field Green functions are used in the calculations and the terms in the time domain Helmholtz-Kirchhoff equation (1) are detailed in the following system of equations (2), where $\cos(\gamma_s) = \frac{(\vec{s}-\vec{r}).\vec{n_S}}{|\vec{s}-\vec{r}|}$ and $\vec{n_S}$ is the normal vector to the measurement surface $(S)$:

$$\begin{cases} G(\vec{s},\vec{r};-t) * \dfrac{\partial p(\vec{s};-t)}{\partial n_s} = \dfrac{1}{4\pi|\vec{s}-\vec{r}|} \times \dfrac{\partial p\left(\vec{s};-t-\dfrac{|\vec{s}-\vec{r}|}{c}\right)}{\partial n_s} \\ \dfrac{\partial G(\vec{r_s},\vec{r};-t)}{\partial n_s} * p(\vec{s};-t) = \dfrac{\cos(\gamma_s)}{4\pi|\vec{s}-\vec{r}|^2} \times p\left(\vec{s};-t-\dfrac{|\vec{s}-\vec{r}|}{c}\right) \\ \qquad\qquad + \dfrac{\cos(\gamma_s)}{4\pi c|\vec{s}-\vec{r}|} \times \dfrac{\partial p\left(\vec{s};-t-\dfrac{|\vec{s}-\vec{r}|}{c}\right)}{\partial t} \end{cases} \tag{2}$$

Equation (1) shows that in order to calculate the time-reversed field $p_{TR}(\vec{r},t)$, the acoustic field must be measured using monopolar and dipolar microphones. In our experiment, the double-layered hemispherical TRM allows to measure both $p(\vec{s},t)$ and its normal derivative using the two probes located at $\vec{s_1} \in (S_1)$ of radius $a_1$ and $\vec{s_2} \in (S_2)$ of radius $a_2$ using first order finite difference schemes:

$$\begin{cases} \dfrac{\partial p(\vec{s};-t)}{\partial n_s} \approx \dfrac{p(\vec{s_1};-t) - p(\vec{s_2};-t)}{a_2 - a_1} \\ p(\vec{s};-t) \approx \dfrac{p(\vec{s_1};-t) + p(\vec{s_2};-t)}{2} \end{cases} \tag{3}$$

Since the acoustic field is not measured on a continuous surface $(S)$ but rather space-sampled on this surface, the surface integral involved in equation (1) is replaced by a discrete sum in order to achieve time-reversal imaging using the measured data on the double-layered hemispherical TRM.

As stated in the previous paragraphs, TR *imaging* is based on the knowledge of the Green functions, which are the propagators in the measurement medium. In free-space-like environments such as an anechoic room, the analytic free-field Green functions are used to back-propagate the measured acoustic field and allow to obtain accurate and satisfying results [11]. This knowledge is also assumed for other methods, such as nearfield acoustic holography and derivatives [14]. However, when the medium is confined or reverberant, there is no analytic knowledge of the Green functions, which degrades the imaging process when not using the right acoustic propagators. This property is the great difference between TR *focusing*, where the back-propagation is achieved in the same medium than the propagation during measurements, and TR *imaging*, where the back-propagation is achieved using a numerical model. Contrary to TR *imaging*, TR *focusing* has been shown to be more efficient in revereberant environments because reverberation enhances the measurement antenna aperture [13, 15]. In order to allow TR *imaging* in confined and reverberant environements, we propose the use of a field separation method (FSM), that separates contributions coming from noise sources inside and outside the region of

interest, thus suppressing the contributions from zones of the steelpan that reside outside the ROI and "dereverberating" the acoustical measurements in order to achieve efficient TR imaging using free-field Green functions.

### 3.2 Field separation method

Previous published works show that separation methods can be used in spherical coordinates in order to recover free-field conditions [10, 16]. The proposed method is based on Weinreich *et al.* work [16] and involves spherical harmonics expansion. Based on the assumption that the TRM lays on a perfectly rigid surface, the pressure fields measured with the double-layered hemispherical antenna can be expressed using even spherical harmonics up to a maximum order N. The maximum order of expansion $N$ is calculated from the number of probes in the TRM. With 36 p-p probes, the maximum order of decomposition is $N = 7$. In equation (4), $Y_n^m(\theta,\phi)$ are the normalized spherical harmonic functions, and $\mathcal{TF}^{-1}$ is the inverse Fourier transform operator:

$$\begin{cases} p(a_1,\theta,\phi,t) = \mathcal{TF}^{-1}\left(\sum_{n=0}^{N}\sum_{\substack{m=-n\\(m+n)\text{even}}}^{+n}\hat{\alpha}_{nm}Y_n^m(\theta,\phi)e^{i\omega t}\right) \\ p(a_2,\theta,\phi,t) = \mathcal{TF}^{-1}\left(\sum_{n=0}^{N}\sum_{\substack{m=-n\\(m+n)\text{even}}}^{+n}\hat{\beta}_{nm}Y_n^m(\theta,\phi)e^{i\omega t}\right) \end{cases} \quad (4)$$

In equation (4), the $\hat{\alpha}_{nm}$ and $\hat{\beta}_{nm}$ are complex coefficients that can be calculated from measured pressures by expansion using orthonormal properties of $Y_n^m$. As shown in equation (5), this formulation can be rewritten in terms of diverging waves (represented by spherical Hankel functions of second kind $h_n^{(2)}$) and standing waves (represented by spherical Bessel functions of first kind $j_n$):

$$\begin{cases} p(a_1,\theta,\phi,t) = \mathcal{TF}^{-1}\left(\sum_{n=0}^{N}\sum_{\substack{m=-n\\(m+n)\text{even}}}^{+n}\left(\hat{a}_{mn}h_n^{(2)}(ka_1)+\hat{b}_{mn}j_n(ka_1)\right)Y_n^m(\theta,\phi)e^{i\omega t}\right) \\ p(a_2,\theta,\phi,t) = \mathcal{TF}^{-1}\left(\sum_{n=0}^{N}\sum_{\substack{m=-n\\(m+n)\text{even}}}^{+n}\left(\hat{a}_{mn}h_n^{(2)}(ka_1)+\hat{b}_{mn}j_n(ka_1)\right)Y_n^m(\theta,\phi)e^{i\omega t}\right) \end{cases} \quad (5)$$

The $\hat{a}_{mn}$ and $\hat{b}_{mn}$ are the complex unknown quantities of the problem, $\hat{a}_{mn}$ being the unknown of interest in our problem in order to achieve dereverberating and denoising of measured pressures on the TRM. Solving this set of linear equations using systems (4) and (5) for $k(a_2 - a_1) \ll 1$ yields: $\hat{a}_{mn} = \frac{ka_1^2}{j(a_2-a_1)} \times \left(j_n(ka_1)\hat{\beta}_{mn} - j_n(ka_2)\hat{\alpha}_{mn}\right)$. The knowledge of the constants $\hat{a}_{mn}$ allows to compute the outgoing fields $p_{out}(a_1,\theta,\phi,t)$ and $p_{out}(a_2,\theta,\phi,t)$ which correspond to the set of data that would have been measured in an anechoic environment and that filter the contribution coming from zones located outside the ROI. These outgoing fields are then taken as entries for the time-reversal imaging process described in the previous subsection. As a consequence, the TR-FSM imaging method allows acoustic imaging of radiating sources in the ROI delimited by the double-layered hemispherical TRM (corresponding to red-coloured notes on Fig.1), and allows to achieve measurements in non anechoic environments without degrading the TR imaging process using free-field Green functions.

## 4 Results and Discussion

In this section, TR-FSM imaging results are first presented in order to test the notes localization reproducibility. We present afterwards the efficiency of the field separation method in suppressing the acoustic radiation contributions coming from outside the ROI and the reverberation effects. Finally, we present and discuss the evidence of coupling and sympathetic vibration that contribute to acoustic radiation from neighbouring notes in the ROI of the steelpan's bowl when a note is struck by the panist. All the figures presented in this section are TR imaging of acoustic intensity computed from the time-reversed RMS pressure on the 1000 points meshed bowl surface with a dynamic of 6 decibels, superimposed onto the photography of notes of the steelpan presented on Figure 1, with the struck note circled in gray.

### 4.1 Notes localization and reproducibility

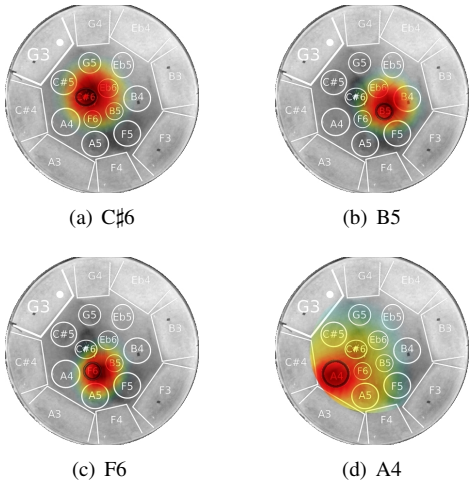


(a) C♯6 (b) B5

(c) F6 (d) A4

Figure 4: TR FSM imaging and localization of radiating sources when struck by panist

Each of the 11 studied notes have been successively struck by the panist with a playing stick. Figure 4 shows the localization of the radiating sources using TR-FSM imaging for 4 different struck notes in the ROI: C♯6, B5, F6, and A4. These 4 struck notes are well localized and show the predominant radiating sources. Each of the 11 studied struck notes have been struck 5 different times. However, for the sake of compactness of the present paper, only one figure per struck note is shown, since the reproducibility of TR-FSM imaging and sources localization is very satisfying with these experiments (correlation criterion $r_c \geq 0.87$ between individual images obtained of 5 experiments on each struck notes, with a confidence p-value $p \leq 0.065$).

### 4.2 Efficiency of field separation method

The field separation method allows to suppress the contribution to acoustic radiation from sources outside the ROI. Figure 5 show the TR imaging without the use of FSM and the TR imaging with the use of FSM for the struck note A5.

Without the use of FSM (Fig. 5(a)), the obtained maps show that the radiatied field is not only originated from A5 which is located in the ROI, but also from the zone of A3,

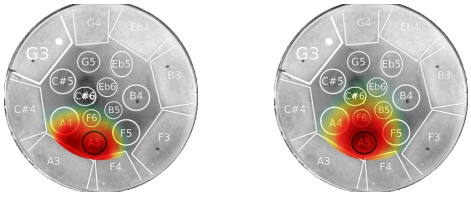

(a) A5 without FSM (b) A5 with FSM

Figure 5: TR imaging and localization of radiating sources when A5 is struck: (a) Without Field separation method - (b) With Field separation method

which can be interpreted in terms of reflections and/or sympathetic and coupled radiating vibrational sources in this adjacent zone of the struck note. When compared to the imaging with the use of FSM (Fig. 5(b)), it appears that FSM efficiently suppresses the radiated field contributions coming from A3, which is located outside the ROI, which confirms the efficiency of this method to focus the imaging process on the region of interest of the instrument.

## 4.3 Evidence of coupled and/or sympathetic vibrations originating acoustic radiation

The studied behaviour of the radiation of the steelpan when A5 is struck in the previous subsection does not allow to determinate whether the radiation contribution coming from the A3 note is originated by simple reflections on the upper part of the bowl or sympathetic/coupled vibrations. However, the study of the TR-FSM imaging of several other notes of the instrument give strong evidences of sympathetic and coupled vibrations of adjacent zones of the struck notes on the instrument that depend on the level of velocity and force of the stick's impact.

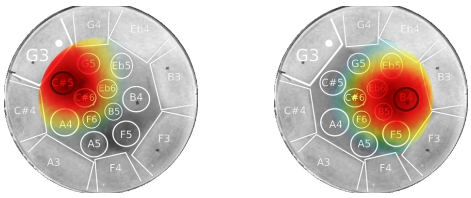

(a) C♯5 (b) B4

Figure 6: TR imaging and localization of radiating sources when (a) C♯5 and (b) B4 are individually struck at high level

Figure 6 shows the imaging obtained when C♯5 and B4 are struck at high level by the panist, exhibiting a zone contributing to the radiation extending to the adjacent notes, especially overlapping the adjacent notes tuned at the octave. This phenomenon can be interpreted as sympathetic and coupling between the notes, since this has only been observed at high level of impact of the stick on the note.

In order to illustrate the fact that this phenomenon depends on strike level, Figure 6 shows the imaging obtained when B4 is struck at low level and high level. When the note is struck at low level (Fig. 6(a)), the resulting TR-FSM imaging only shows that the struck note is the predominant radiating source, on contrary to the situation where the note is struck at high level (Fig. 6(b)), where adjacent notes seem to contribute to radiation.

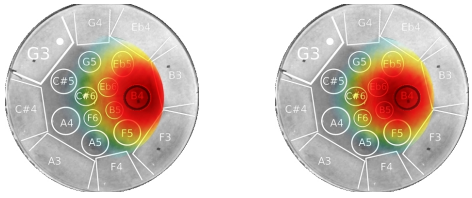

(a) B4 struck at low level (b) B4 struck at high level

Figure 7: TR imaging and localization of radiating sources when B4 is struck (a) at low level (b) B4 at high level

Interestingly, this sympathetic/coupling phenomenon has been strongly observed when F5 was struck by the panist. In this situation, as shown on Figure 7, the vibration transfer and coupling between notes is so strong, that after TR-FSM imaging, the predominant radiating source observed is not the struck note, but rather one of its adjacent note, whose pitch corresponds to the octave above the struck note's pitch.

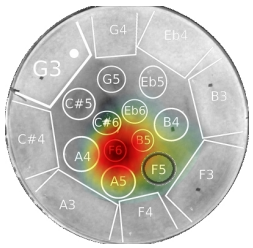

Figure 8: TR imaging and localization of radiating sources when F5 is struck: the predominant radiating source corresponds to F6 which is tuned at an octave above F5

This phenomenon has been observed for each of the 5 successive experiments on this struck notes, which gives confidence on the observed results and corroborates previous published studies [1] [3] [5] [9]. Its observation using acoustic measurement also gives experimental evidence of coupling between notes using acoustic radiated field measurements. On contrary to vibrational measurements previously published by several authors, this experiment shows that the sympathetic/coupled vibration can give rise to situations where the predominant radiating note is not the struck note. This result gives interesting perspectives for the study of this modern instrument considering coupling and acoustic radiation, and gives part of an explanation to the strong acoustic signature of this instrument.

The fact that the predominant radiating source in this experiment is not the struck note may be explained in the following way: the frequency of F5's second vibrational mode is tuned to the frequency of the first vibrational mode of F6. As a consequence, this situation is ideal for sympathetic vibration, thus allowing parametric internal resonances between these two notes. As the second vibrational mode of F5 corresponds to a vibrational dipole and the first vibrational mode of F6 corresponds to a monopole, the acoustic radiation of the first vibrational mode of F6 is more efficient than the acoustic radiation of the second vibrational mode of F5. However, the first vibrational mode of F5 should be radiating acoustically, but it seems that its attenuation over time is so high that F6 radiates more than F5 when F5 is struck.

One of the advantages of time-reversal techniques is that it gives access to time-domain evolution of the pressure field.

As a consequence, one can compute the pressure level imaging using TR-FSM imaging for several time windows, thus allowing to observe the evolution of the vibrational transfer from the struck note to the adjacent notes that justify the previous assumption. This computation has been done on Figure 8, with 3 time windows, showing that F5 rapidly extinguish in terms of radiation and that after a time of approximately 100 ms, the predominant radiating source is F6:

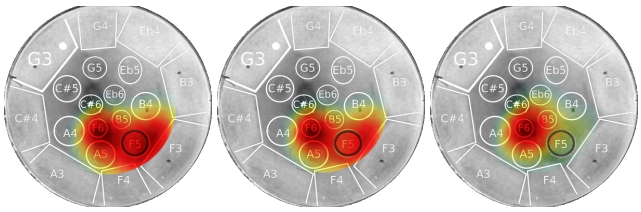


(a) F5 , 62.5 ms window (b) F5, 93.75 ms window (c) F5, 125 ms window

Figure 9: TR imaging and localization of radiating sources when F5 is struck with several time windowing for acoustic level computation: (a) 62,5 ms - (b) 93,75 ms - (c) 125 ms

# 5 Conclusions

This study shows that TR-FSM is a powerful method for the imaging and localization of sound sources on a double-second steelpan, allowing to assess the radiation of sources in a restricted area of the steelpan's bowl, without being perturbated by other radiating sources. Furthermore, thanks to the proposed field separation method, these measurements have been achieved in a reverberating environment without perturbing the results. The imaging method shows a great precision in sources localization and reproducibility and the obtained results allowed to observe coupling and sympathetic vibrational behaviours contributing to acoustic radiation of the instrument. Interestingly, this phenomenon is observed when the panist strikes the instrument at high level. Some of the results gave insight of the coupled/sympathetic vibrations originating acoustic radiation, even showing that for a particular note, the zone that predominantly radiates acoustic energy was not the struck note but rather its adjacent note whose pitch was tuned to the above octave. TR-FSM imaging also allowed to have access to the time evolution of localization of radiating sources. This study may be completed in future works by further investigations using TR-FSM or other imaging methods such as the data completion method, and using a larger TRM allowing to image all of the notes included in the instrument's bowl.

# Acknowledgments

The authors would like to greatly thank Calypsociation who lent the studied steelpan and made this study possible.

# References

[1] T.D Rossing, U.J Hansen, D.S Hamton, "Vibrational mode shapes in Caribbean steelpans. I. Tenor and double second", *J. Acoust. Soc. Am.* **108**(2), 803-812 (2000)

[2] L.E Murr, E.V Esquivel, A.A Bujanda, N.E Martinez, K.F Soto,A.S Tapia,S. Lair,A.C Somasekharan, "Metallurgical and acoustical comparisons for a brass pan with a Caribbean steel pan standard", *J. Mater. Sci.* **39**, 4139-4155 (2004)

[3] D. S. Hampton, C. Alexis, T. D Rossing, "Note coupling in Caribbean steel drums", *J. Acoust. Soc. Am.* **82**, S68 (1987)

[4] T. D Rossing, D. S. Hampton, U.J Hansen , "Music from oil drums: The acoustics of the steelpan" *Phys. Today* **49**, 24–29 (1996)

[5] A. Achong, K.A Sinanan-Singh, "The steelpan as a system of mode-localized oscillators, Part II: Coupled subsystems, simulations, and experiments", *J. Sound Vib.* **203**, 547-561 (1997)

[6] B. Copeland,, T. D Rossing, A. Morrison, "Sound radiation from Caribbean steelpans"*J. Acoust. Soc. Am.* **117**(1), 375–383 (2005)

[7] F. Muddeen, B. Copeland, "Sound radiation from Caribbean steelpans using nearfield acoustical holography", *J. Acoust. Soc. Am.* **108**(2), 1558-1565 (2012)

[8] A. Achong, "The steelpan as a system of nonlinear mode-localized oscillators, I: Theory, simulations, experiments and bifurcations", *J. Sound Vib.* **197**, 471–487 (1996)

[9] T. Woods, P.F. O'Malley, J.F. Vignola, J. Judge, "Surface normal measurement of Caribbean steelpan vibration", *Proc. of Meetings on Acoustics, NOISE-CON*, **9**, p.035003 1-10

[10] M. Melon, C. Langrenne, P. Herzog, A. Garcia, "Evaluation of a method for the measurement of subwoofers in usual rooms," *J. Acoust. Soc. Am.* **127** (1), 256–263 (2010)

[11] E. Bavu, A. Berry, "Super-resolution imaging of sound sources in free field using a numerical time-reversal sink", *Acta Acust. United Ac.*, **95** (4), 595-606 (2009)

[12] S.G. Conti, P. Roux, W.A. Kuperman, "Near-field time-reversal amplification", *J. Acoust. Soc. Am.* **121** (6), 3602–3606 (2007)

[13] M. Fink, D. Cassereau, A. Derode, C. Prada, P. Roux, M. Tanter, J-L. Thomas, F. Wu, "Time reversed acoustics", *Rep. Prog. Phys.* **63**, 1933-1995 (2000)

[14] S. F. Wu, "Methods for reconstructing acoustic quantities based on acoustic pressure measurements", *J. Acoust. Soc. Am.* **124** (5), 2680-2697 (2008)

[15] E. Bavu, C. Besnainou, V. Gibiat, J. de Rosny, M. Fink, "Subwavelength Sound Focusing Using a Time-Reversal Acoustic Sink", *Acta Acust. United Ac.* **93** (5), 706-715 (2007)

[16] G. Weinreich, E. B. Arnold, "Method for measuring acoustic radiation fields", *J. Acoust. Soc. Am.* **68**, 404–411 (1980)